2019-12

AERATION EFFECTS ON WATER-STRUCTURE IMPACTS: PART 1. DROP PLATE IMPACTS

Tri, M

10.1016/j.oceaneng.2019.106600
Ocean Engineering
Elsevier

AERATION EFFECTS ON WATER-STRUCTURE IMPACTS: PART 1. DROP PLATE IMPACTS

T. Mai [a, b, 1], C. Mai [c], A. Raby [a] and D. M. Greaves [a]

[a] *School of Engineering,, University of Plymouth, Plymouth, Devon, PL4 8AA, United Kingdom*
[b] *Now at National University of Civil Engineering, 55 Giai Phong, Hai Ba Trung, Hanoi, Vietnam*
[c] *Thuy Loi University, 175 Tay Son, Dong Da, Hanoi, Vietnam*

ABSTRACT

Current offshore engineering design codes for wave loading are based on pure water, but wave impacts often involve aerated flow, either as a result of air entrapment as the wave overturns or due to impact with a wave that is already broken. Therefore, it is necessary to develop a new understanding of how design codes should incorporate water-air mixture for wave impact. This experimental study investigates aeration effects on wave impacts by means of slamming impacts of a square flat plate onto a pure and aerated water surface, with zero degree dead-rise angle. The (low) aeration level between 0% and 1.6% was applied and the drop velocity varied from about 1 m/s to 7 m/s. There was a significant reduction in the peak impact loads (both pressure and force) for impact in aerated water compared to that in pure water. There was also a significant reduction in the first phase of the pressure and force impulse for aerated water. The variation in impulsive loadings is less sensitive than peak loadings for impacts. The implication for design is that maximum instantaneous loads may be conservative in the presence of aerated water.

Keywords: aeration effect, slamming, wave impact, physical model

1 Introduction

Hydrodynamic impact problems are frequently encountered in marine engineering (Faltinsen, 1993 & 2000; Kapsenberg, 2011), water sports (Rubin, 1999) and natural hazards (Kay, 2014; Rodgers & Bryson, 2014). Slamming of high speed marine vessels on the water surface and ship bows subject to wave impact both require the loading to be taken into account for practical design of these structures. In addition, the ditching of an aircraft on the water surface is another problem of water slamming on a body which can lead to damage to the aircraft and potential loss of life. Hydrodynamic impact and slamming is a complicated process in which air cushion, air bubbles, compressibility of the water and hydroelasticity may be relevant (Faltinsen et al., 2004). Water slamming has been investigated over several decades using both theoretical and physical models. Von Kármán (1929) developed the first theory to estimate pure water impact for a wedge and then for a horizontal plate. In 1932, Wagner (1932) developed theory for a wedge with very small dead-rise angle, small enough not to trap air under impact. Several experimental studies have been undertaken to investigate water slamming by dropping a wedge (Chuang, 1966a; Zhu, 1995; Zhao et al., 1997), a horizontal-bottomed body (Chuang, 1966b; Verhagen, 1967; Zhu, 1995; Faltinsen, 2000; Bullock et al., 2001; Kwon et al., 2003; Ermanyuk et al., 2005; Oh et al., 2009), a horizontal circular cylinder (Lange and Rung, 2011; Van Nuffel et al., 2014) and a pyramid onto a still pure water surface (Alaoui et al., 2012 & 2015). Furthermore, Smith et al. (1998) conducted a series of drop tests of a horizontal plate onto waves of different steepness.

If water is assumed to be compressible, then the peak pressure at the instant of impact of a horizontal plate onto still water is equal to the acoustic pressure (von Kármán, 1929) $p_a = \rho c v$, where ρ is the fluid density, c is the speed of sound in the fluid and v is the plate velocity just before impact (also

[1] Corresponding author.

E-mail address: tri.mai@plymouth.ac.uk, trimc@nuce.edu.vn (Tri Mai)

known as the impact velocity). In practice, the maximum acoustic pressure never occurs, because an air layer is trapped between the flat plate and the water surface and this air acts as a cushion (Chuang, 1966a&b; Lewison and Maclean, 1968). In the experiment of Chuang (1966a&b) the maximum impact pressure is found to be proportional to $\rho c_a v$, where c_a is the speed of sound in air rather than in water. In the theory developed by Chuang (1966a&b), the compressibility of both the air and water was considered in a general solution of the problem. However, because the maximum impact velocity was limited to 1.92 m/s, the finding in Chuang's tests may not necessarily apply to higher impact velocities ($v > 1.92$ m/s). On the other hand, the compressibility of the water is neglected by Verhagen (1967) because the events of interest are expected to occur in a timescale of the order required by an acoustic wave in air to travel over a distance l, i.e., $\Delta t = l/c_a$, which is large compared with l/c (l is the half width of the flat plate). Verhagen's experiments indicated that this assumption is justified; however, the experiments were limited to small values of the mass of the body compared with the added mass. Verhagen (1967) found that the maximum impact pressure was proportional to the square of the impact velocity for small values of $M/\rho l^2 = 0.5$, but this relationship was linear if $M/\rho l^2 >> 1$ (M is the mass per unit length of the impact plate). Zhu (1995) found that the slamming pressure coefficient, $C_p = p_{\max}/(0.5\rho v)$, increases with the weight of the model due to the added mass of water, where p_{max} is the peak slamming pressure. The coefficient of weight has been defined at $C_m = m/A$, where m is the weight of the model and A is the flat impact area. It was found that there was a considerable amount of scatter in the peak slamming pressures, but the pressure impulses of the first positive phase (the duration over which the pressure starts to rise up to the peak and then falls down to zero in the pressure time history under impact) were more or less the same (Zhu, 1995).

In open oceans and seas, bubbles are known to be created in the upper ocean through different mechanisms (Deane and Stokes, 1999), such as: (i) the action of breaking gravity and capillary waves (Longuet-Higgins, 1993); (ii) rain drop impact on the ocean surface (Franz, 1959; Pumphrey and Elmore, 1990) and (iii) melting snow (Blanchard and Woodcock, 1957). However, most bubbles near the ocean surface are caused by breaking waves under moderate wind conditions (Medwin, 1977; Dean and Stokes, 1999). The entrained bubbles in both field and laboratory have diameters of the order of millimetres and the rise velocity of those bubbles is nearly constant for bubble diameters ranging from 0.5 to 50 mm (Chanson et al., 2002; Chanson, 1997; Wood, 1991). A burst of sound is emitted at a frequency approximately given by Minnaert's equation after a bubble is first formed (Deane and Stokes, 1999; Minnaert, 1933). Bubbles produced by breaking waves are concentrated within a plume and this plume starts to dissipate through the processes of dissolution, diffusion, and degassing (Deane and Stokes, 1999). According to Monahan (1993), there are different phases of a bubble plume's life cycle, namely the α-plume, β-plume and γ-plume. The α-plume is the phase of a plume formed when most bubbles are created by breaking waves. In the open ocean, breaking waves may be caused by constructive interference, wave-wave, wave-current and wind-wave interactions (Melville, 1996). This α-plume persists for seconds and is characterised by high void fractions (of order 10%) and a broadband spectrum of bubble sizes (tens of microns to millimetres); see Monahan (1993) and Deane and Stokes (1999). Once the momentum of the combination of the downward moving jet and breaking wave is dissipated, the most diffuse bubbles aggregate and then form the β-plume. As time moves on, the largest bubbles rise to the surface, the remaining smaller bubbles are spread by turbulent diffusion over a greater volume, which is represented by the γ-plume (Monahan, 1993).

Firstly, the influence of air in the water (both entrapped pockets and entrained bubbles) is known to lead to variability in wave impact pressures and forces. There are limited experimental studies of slamming impact in aerated water (Bullock et al., 2001; Lange and Rung, 2011), and design codes for wave impact on offshore structures and ships are all based on pure water environments (Det Norske Veritas, 2012, 2014 & 2016). Here, we investigate the effects of aeration on wave impact and assess whether design practice needs to adapt to take these effects into account. The effect of aeration on wave impact has been investigated through two linked experiments: first, by dropping a flat plate from various heights onto the surface of water aerated to various degrees presented in this paper;

second, by generating wave impacts of different types on a truncated vertical wall (representing a section of FPSO, Floating Production Storage and Offloading vessel, hull) in pure and aerated water, which will be presented in a companion paper Aeration effects on water-structure impacts: Part 2. Wave impacts on a truncated vertical wall.

2 Methodology

2.1 Physical model of drop test

The experimental work for the drop tests was carried out in the Ocean Basin at the University of Plymouth COAST Lab. The Ocean Basin is 35 m long by 15.5 m wide and has a movable floor that allows operation at different water depths up to 3 m. For these tests the depth was set to 1m. The falling block included a rigid impact plate connected to a carriage constructed from two driver plates with a total mass that could be varied from 32 kg to 52 kg. The block dropped through a 4 m high vertical guide frame fixed on the gantry crossing over the basin (see Figure 1a,b). The impact plate was 0.25 m long, 0.25 m wide and 0.012 m thick, and the impact velocity varied between 1 m/s and 7 m/s depending on the drop height. Pressures on the bottom surface of the impact plate were measured by five miniature pressure transducers (FGP Sensors XPM10) with 8 mm head diameter and a measurement range of up to 100 bar, installed at various locations on the impact plate (Figure 1c). The impact velocity was integrated from accelerations obtained from an accelerometer (Model 4610) with a range of up to 200g, in which g is the acceleration due to gravity, mounted on the top surface of the impact plate. The sampling frequency was 50 kHz for pressure transducers, accelerometer and displacement sensors. Table 1 lists the drop test conditions.

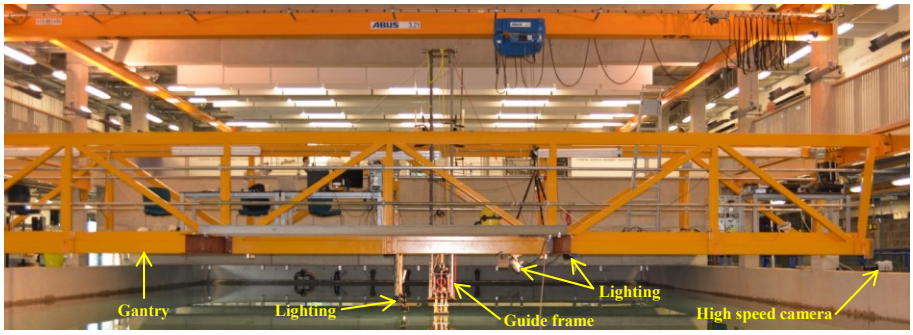

(a)

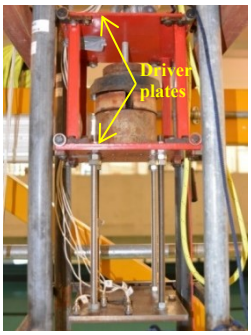

(b)

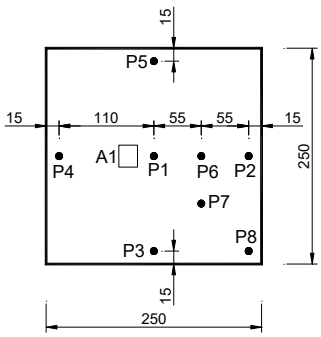

(c)

Figure 1: (a) Overview of drop test rig in the Ocean Basin; (b) Carriage and falling block; (c) Configuration of the instrumentation on the plate. The units are in mm. 'P' and 'A' represent pressure transducer and accelerometer respectively.

Table 1: Drop test conditions.

Total plate mass	**Aeration levels**			
(kg)	0	0.8 %	1 %	1.6 %
32	v = 4-7m/s	v = 4 - 7 m/s		
52	v = 1-7m/s			

2.2 Evaluation of pure water in the Ocean Basin

The assumption of 'pure' water, i.e. water in the absence of submerged air, in the Ocean Basin was evaluated by measuring the speed of sound in the water using an Acoustic Systems Trainer for SONAR (SOund NAvigation and Ranging). The speed of sound in the water had a mean value of 1471.90 m/s and standard deviation of 0.69 m/s, based on 14 measurements after the water surface was completely calm. This measured speed of sound is about 99.74 % of the theoretical estimation value of 1475.79 m/s for pure water at 22ºC (according to Wilson, 1960).

After each drop test in pure water, 15 minutes was allowed for the water surface to become calm again before the next test. According to Stokes' theory (Detsch and Harris, 1989; Leger-Belair et al., 2000), a bubble of diameter 0.05 mm needs about 12.26 minutes to rise through a water depth of 1 m as used in the drop test, and this bubble is degassed at the water surface. Stokes' theory and the experimental data obtained by Leger-Belair et al. (2000) show that the rise velocity is proportional to the bubble radius. Therefore, after each test all bubbles of diameter larger than 0.05 mm would have risen to the water surface and the water degassed during the interval between tests.

2.3 Bubble generation and void fraction estimations

In this study, aerated water was achieved using a bubble generation system made of a clear perspex box with a perforated square top-plate (dimensions of 0.54 x 0.54 x 0.002 m), placed at a depth of 1 m in the Ocean Basin. Holes of 0.2 mm diameter were created in the plate using a laser cutter. The holes were uniformly distributed over a square area of 0.495 x 0.495 m^2 with a hole spacing of 10 mm. To generate aerated water, air from a compressor was injected into the bubble generator via four inlets. Snapshots of the aerated water generated by different injection air pressures are presented by Mai et al. (2014), Ma et al. (2016) and Mai (2017), which clearly show that the bubble density increases with injection pressure. Injecting air pressures of 0.065 bar, 0.083 bar and 0.137 bar into the bubble generator, produced void fractions of 0.8 ± 0.31 %, 1 ± 0.39 % and 1.6 ± 0.07 % which were calibrated by a volumetric method at a depth of 25 cm from the water surface (Figure 2) (see Mai, 2017 for more details).

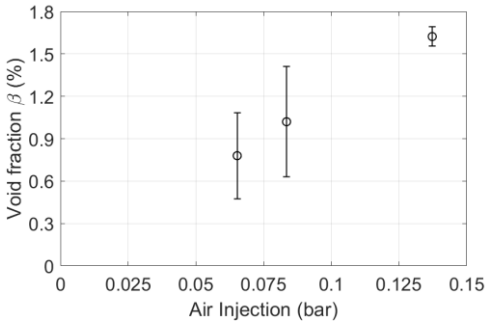

Figure 2: Void fraction calibrated in the Ocean Basin applying the volumetric method. Mean values are shown, with error bars representing the standard deviation of nine measurements.

3 Results and discussion

3.1 Slamming in pure water

Figure 3 presents motion time histories for impact of a 52 kg plate in pure water at 7.21 m/s impact speed. Time $t = 0$ s corresponds to the time of maximum force. The maximum acceleration due to the impact was not captured by the 200g accelerometer as the signal was clipped from the moment that the plate hit the water surface (Figure 3a). Figure 3b shows that the velocity is zero at the start of the test and then increases linearly during the free fall of the impact plate until a maximum velocity is obtained. At the instant of reaching its maximum velocity, the impact plate starts to decelerate and this corresponds to first contact with the water surface. The velocity of the impact plate fluctuates for about 30 milliseconds, then decreases smoothly to zero and changes its direction due to the safety rope, which was connected to the carriage and used to stop the carriage from leaving the guide frame. Figure 3c shows the integrated displacement of the impact plate during the test.

Figure 4 presents the measured pressures and the integrated force (F) during impact for the test case presented in Figure 3. At impact, pressures start to increase up to the maximum values. The maximum pressure at the centre of the impact plate (P1) is much higher than near the edges (P2 & P8) and slightly higher than the maximum pressures at locations P6 & P7 located near the plate centre. The maximum pressures are attained at time instants between 1.24 ms and 1.32 ms after first contact between the impact plate and water surface. It is observed that the maximum pressure at location P8 is always attained earlier than the maximum pressure P1 at the centre of the plate, by between about 0.08 ms under impact velocity v = 7.21 m/s and 0.38 ms under impact velocity v = 1.33 m/s. This was also observed by Lewison and Maclean (1968) and is explained by a phenomenon called *coalescence* in which the air and water merge to form effectively a single phase. Coalescence occurs after the peak pressure at any location on the impact plate and it occurs later relative to the pressure peak at the edge of the plate than at the centre.

A second pressure peak is observed under high impact velocities (v = 5.5 m/s to 7.21 m/s), at between 0.66 ms and 0.6 ms after the first peak (see Figure 4). The second pressure peak may be due to the propagation of an acoustic shock wave travelling either through air to the edge of the plate and back, over a distance $2l$, where l is the half width of the impact plate, or through water to the bottom of the basin and back, over twice the tested water depth, $2h$. The time-scale associated with propagation of the shock wave in water, namely $2h/c_w$ is 1.36 ms, where the measured speed of sound in pure water is c_w = 1471.90 m/s, whereas the propagation time needed for the shock wave travelling in air, $2l/c_a$ is 0.74 ms, where the speed of sound in air is taken to be c_a = 340 m/s. Based on these calculations, the second scenario of the shock wave travelling through the air gap along the width of the plate and back seems most plausible because the time-scale is comparable to the observations (0.6 ms to 0.66 ms), and the horizontal half-size of the trapped air region is less than l. Unfortunately, the trapped air region cannot be observed in sufficient resolution from the low frequency underwater cameras (frame rate of 25 - 30 fps) used in this experiment.

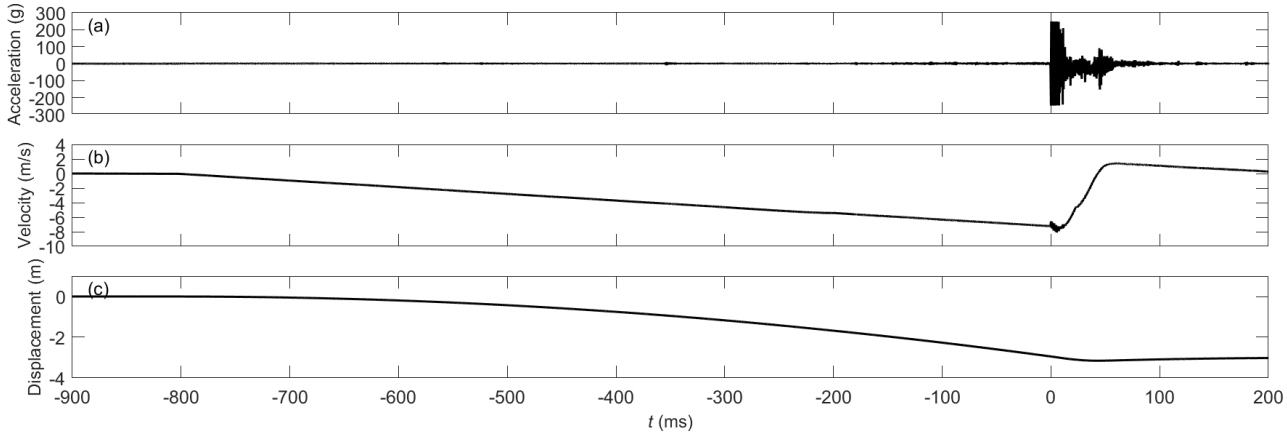

Figure 3: Typical time-histories of acceleration, velocity and displacement of a test in pure water (v = 7.21 m/s, m = 52 kg).

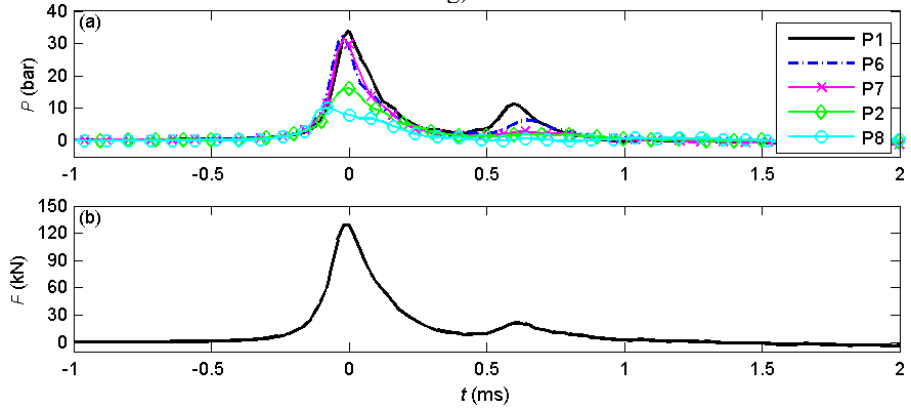

Figure 4: Typical time-histories of pressures and force of impact in pure water (v = 7.21 m/s, m = 52 kg).

Distinct post-impact pressure oscillations have been observed and depicted in Figure 5 for tests involving impact velocities of 1.33 m/s, 4.28 m/s and 7.21 m/s. The left-hand plots (Figure 5a, c, e) are the time histories of pressures and the right-hand plots (Figure 5b, d, f) are the respective Fast Fourier Transforms (FFTs). The pressure oscillations at the central point (P1) and near the plate centre (P6) are much more obvious than near the edges of the plate (P2) at all impact velocities. The evolution of the impact pressure loading comprises distinct stages: the first shock loading, fluid expansion loadings (under atmosphere pressures) and re-loadings. This evolution of pressures due to impacts in pure water at high velocities (v = 5.5 m/s to 7 m/s) was also observed in the numerical simulations by Ma et al. (2016).

The natural frequency of the falling block, carriage and support frame set-up is about 500 Hz, and so is not likely to be the cause of the observed oscillation frequencies, which vary from 139.9 Hz to 319.7 Hz. These oscillations in pressure may be due to repeated compressions and expansions of the trapped air when the impact plate is about to hit the water surface (Verhagen, 1967; Lewison and Maclean, 1968) and/or due to reflection of the acoustic shock wave from the bottom of the basin (Lange and Rung, 2011). The time required for pressure wave transmission through twice the water depth is about 1.35 ms as calculated above, which corresponds to a frequency of 740 Hz. Under an impact velocity of 1.33 m/s, the peak frequency of the oscillations is 319.7 Hz. Under impact velocities of 4.28 m/s and 7.21 m/s, the peak frequencies of oscillations are approximately the same at 139.9 Hz. These frequencies of oscillation are all much smaller than that calculated for the sound wave reflecting from the basin floor and so this is unlikely to be the cause of the oscillations in pressure. Table 2 presents the oscillation frequencies and their corresponding oscillation periods under different impact velocities. In addition, bubble sizes estimated from the oscillation frequencies applying Minnaert's equation (Minnaert, 1933) are also presented. It is shown in Figure 5 and Table 2 that as the impact velocity is increased, the frequency of these pressure oscillations reduces and the bubble size for a corresponding oscillation is increased. This suggests that the trapped air bubble, if this is indeed the effect being measured, is larger for higher impact velocity. As mentioned above, it is not possible to observe the trapped air bubble clearly in the underwater camera footage, but the size of trapped air bubble predicted by the theory is consistent, being of the order of the size of the plate.

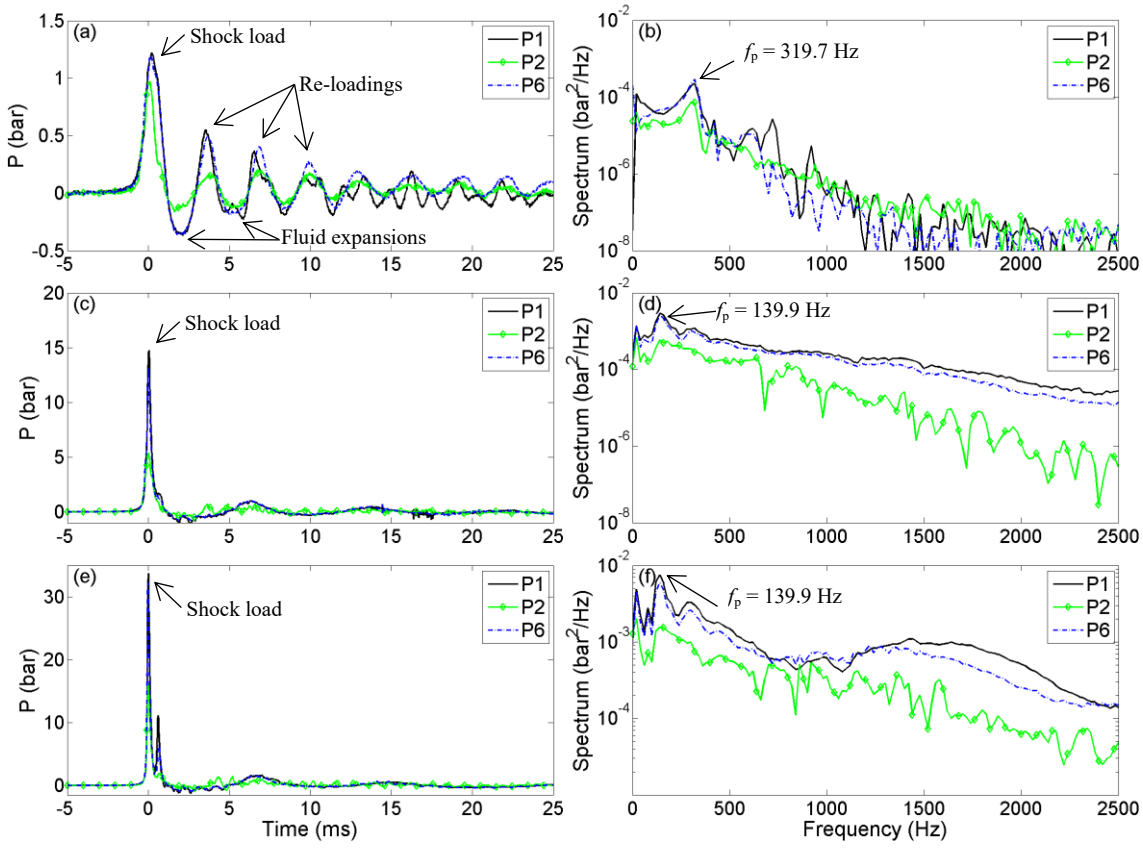

Figure 5: Oscillations in pressure (left plots) and their spectra (right plots) under impact in pure water: (a, b) v = 1.36 m/s; (c, d) v = 4.28 m/s; (e, f) v = 7.21 m/s. Mass of the plate m = 52 kg. Note that the vertical scales are different.

Table 2: Distinct post-impact pressure oscillation frequencies and associated periods and bubble diameters.

v (m/s)	f (Hz)	T (ms)	D_{bubble} (Minnaert, 1933) (mm)
1.36	319.7	3.13	20.5
4.28	139.9	7.14	46.8
7.21	139.9	7.14	46.8

For structural design, it is essential to understand the maximum environmental load condition. By determining the distribution of maximum pressures on a plate, the local loads and hence any requirement to strengthen parts of the plate can be established, for applications such as the design of a hull of a ship, the bow of a ship, or the hull of an FPSO. Spatial 2D-distributions of the maximum pressures on the square plate have been obtained from the available measured pressure points P1-P8 on the plate using linear integration from the measured data points, which are represented by the dots shown in Figure 6. In Figure 6, an 0xy plane coordinate system is applied on the surface of the impact plate, with the plate centre at (x/a, y/a) = (0, 0) and a is the half width of the plate. The largest maximum pressure always occurs at the centre of the plate. In Figure 6b-f, the pressure distribution has similar characteristics whereby the pressure reduces to 80% of its maximum value at the mid point and 40% at the edge. The lowest impact velocity of v = 1.34 ± 0.02 m/s has a different distribution with more uniform pressure (Figure 6a).

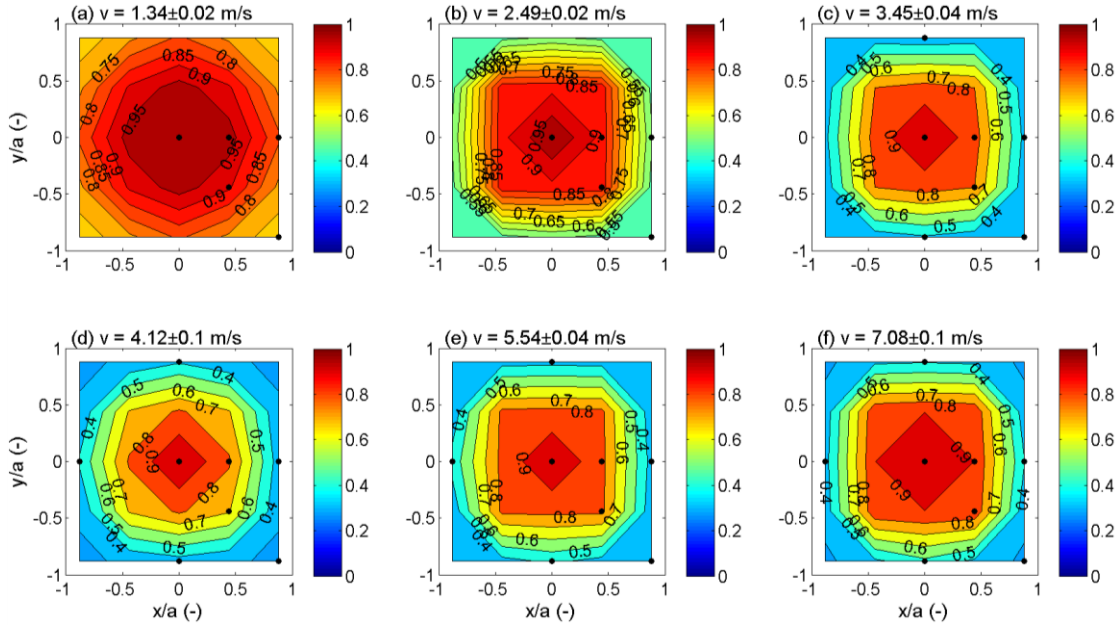

Figure 6: Spatial distribution of dimensionless maximum impact pressure (P_{imax}/P_{1max}) on the 52 kg plate in pure water for a range of impact velocities. P_{1max} is the maximum impact pressure at the centre of the plate and P_{imax} represents all locations on the plate surface.

Figure 7 presents both the maximum pressure P1 measured at the centre of the impact plate and the maximum integrated force F plotted against the impact velocity, for the tests in pure water with the plate mass of 32 kg and 52 kg. In each plot of Figure 7, the circles represent the experimental maximum pressures (Figure 7a,c) or maximum force (Figure 7b,d) and the solid line represents fitted curves with functions as follows.

For pressure:

$$P_{\max} = a_P v^2 , \qquad (1)$$

or force:

$$F_{\max} = a_F v^2 , \qquad (2)$$

where the empirical coefficients a_P and a_F are estimated by the non-linear least-squares algorithm in Matlab to obtain the best curve fit to the experimental data. Empirical coefficients a_P, a_F and the correlation coefficient R^2 are presented within Figure 7. For the larger mass in particular (Figure 7c,d) it is evident that the impact pressure and force are proportional to the square of the impact velocity. For the present experiment with $M/\rho l^2 = 8.2$ (for $m = 32$ kg) and 13.3 (for $m = 52$ kg), this relationship of the impact pressure and impact velocity is expected to be linear according to the numerical investigation by Verhagen (1967) for the case with $M/\rho l^2 >> 1$. The theoretical formulae proposed by von Kármán (1929) and Chuang (1966) are also included in Figure 7 for comparison. Experimental results of the present study are much lower than the acoustic pressure estimation (von Kármán, 1929), are similar to Chuang's (1966) theory at low velocities and much higher at high impact velocities. This may be because Chuang's theory was validated experimentally for impact velocities up to 1.92 m/s only, and so might not be appropriate to apply to the high impact velocities in the range of 2 m/s and 7 m/s tested in the present study. The empirical coefficient a_P is between 0.75 to 0.79 and can be converted into impact coefficient ($C_p = P_{max}/\rho v^2$) with a range of 75 to 79. The impact coefficient presented here is much higher than the range of 0.6 to 9.7 found in Chuang et al. (2017) and the range of 3 to 21 of Chan (1994)..

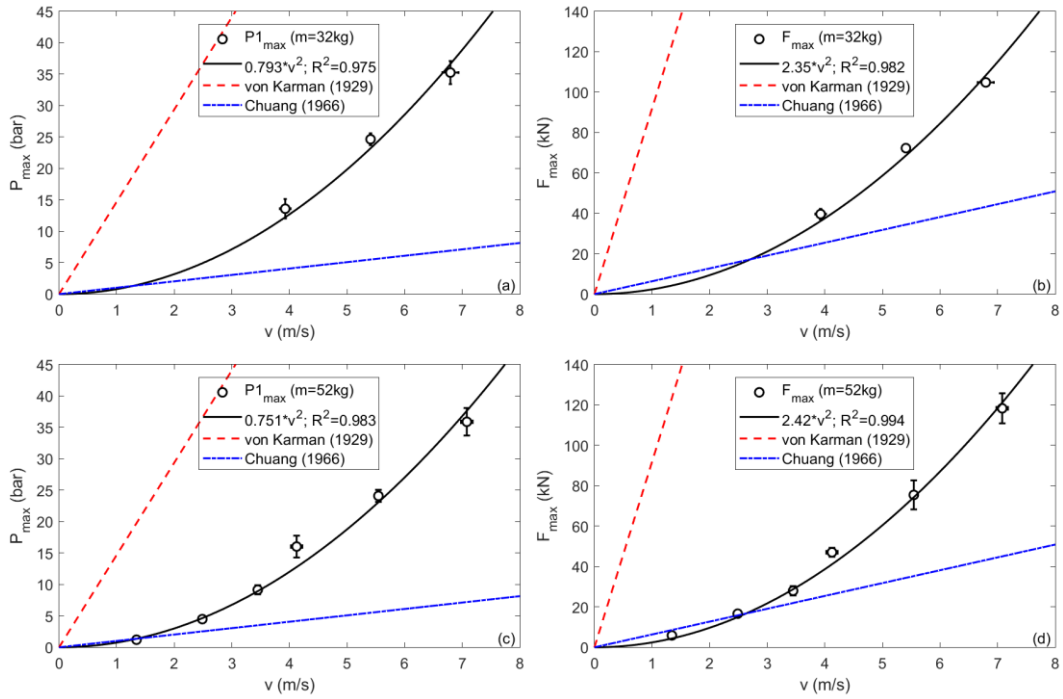

Figure 7: Impact pressure ($P1_{max}$) and force versus impact velocity in pure water: (a,b) $m = 32$ kg; (c,d) $m = 52$ kg. Error bars represent the standard deviation of the repeated tests.

3.2 Slamming in aerated water

Figure 8 shows the measured acceleration, the integrated velocity and displacement of a plate impact in aerated water with void fraction of 1.6%. The impact velocity was 7 m/s and the plate mass was 52 kg. The plate acceleration in aerated water (Figure 8a) is much less than in pure water (Figure 3a). The velocity of the plate decreases smoothly after the plate makes contact with the water surface (Figure 8b) and the velocity trace after impact is found to be less complex than the impact in pure water presented in Figure 3b. The displacement trace of the impact plate in aerated water (Figure 8c) looks identical to the one for impact in pure water (Figure 3c).

The water surface becomes unstable as it is disturbed by the bubble generation, and this is expected to affect the pressure traces. The measured pressures P1-P5 and integrated force are presented in Figure 9. Peak pressures occur at different instances in time, separated by a few milliseconds (Figure

9a). In this case, the impact pressure and force in aerated water are much lower than those in pure water in Figure 4, i.e. peak pressure reduced from about 36 bar in pure water to 6 bar in aerated water - about one order of magnitude reduction. This reduction is due to the presence of air in water and may also be due to the water surface distortion which leads to the deadrise angle of the impact increasing. Similar reductions in impact pressure in aerated water were also found in experimental studies on drop tests of a circular plate by Bullock et al. (2001) and a cylinder at deadrise angle of 0° by Lange and Rung (2011).

Figure 10 presents the pressure traces after impact of the 52 kg plate in aerated water (β = 1.6 %) with impact velocities of 4.12 m/s and 7 m/s. There is no distinct oscillation of pressures after the impact in aerated water (Figure 10a,c) as was observed from the impact in pure water (Figure 5a,c,e). There seems to be only quasi-hydrostatic pressure after the impact in aerated water. The associated pressure amplitude spectra are presented in Figure 10b,d and there is no high frequency peak as was observed in pure water due to the trapped air between the plate and water surface.

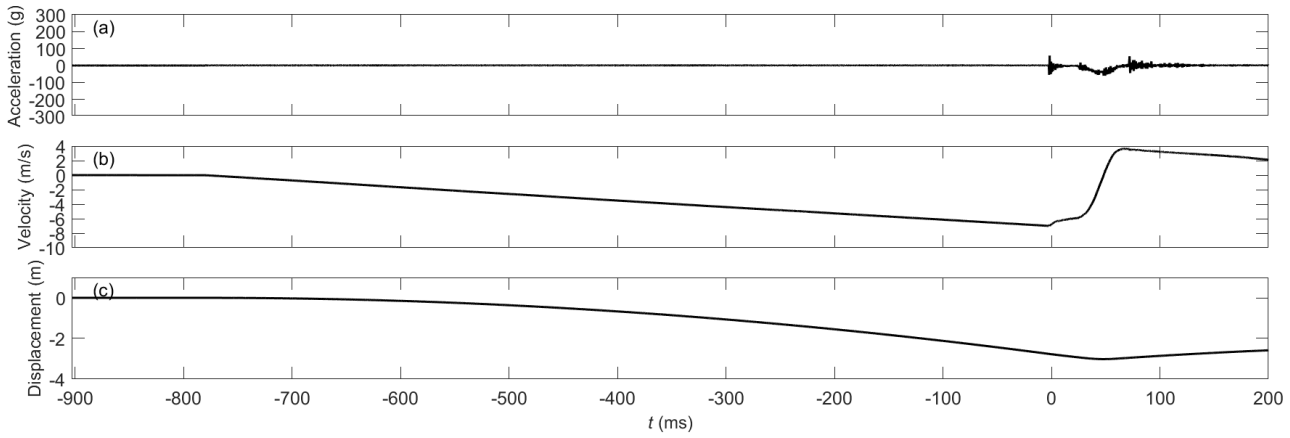

Figure 8: Typical time-histories of acceleration, velocity and displacement of a test in aerated water β = 1.6 % (v = 7 m/s, m = 52 kg).

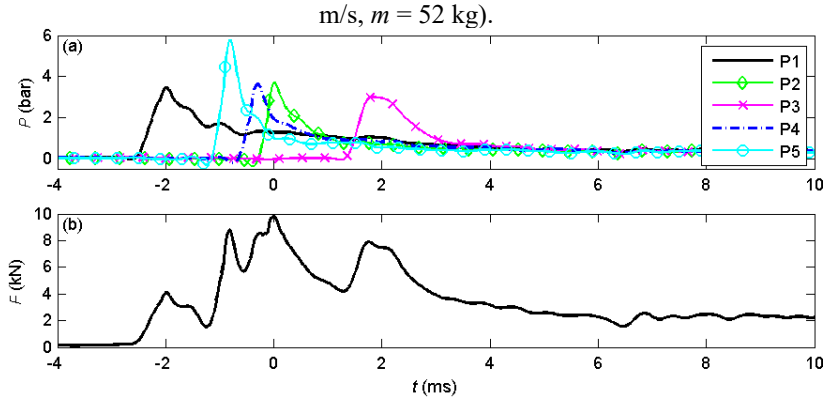

Figure 9: Typical time-histories of pressures and force around impact in aerated water β = 1.6 % (v = 7 m/s, m = 52 kg).

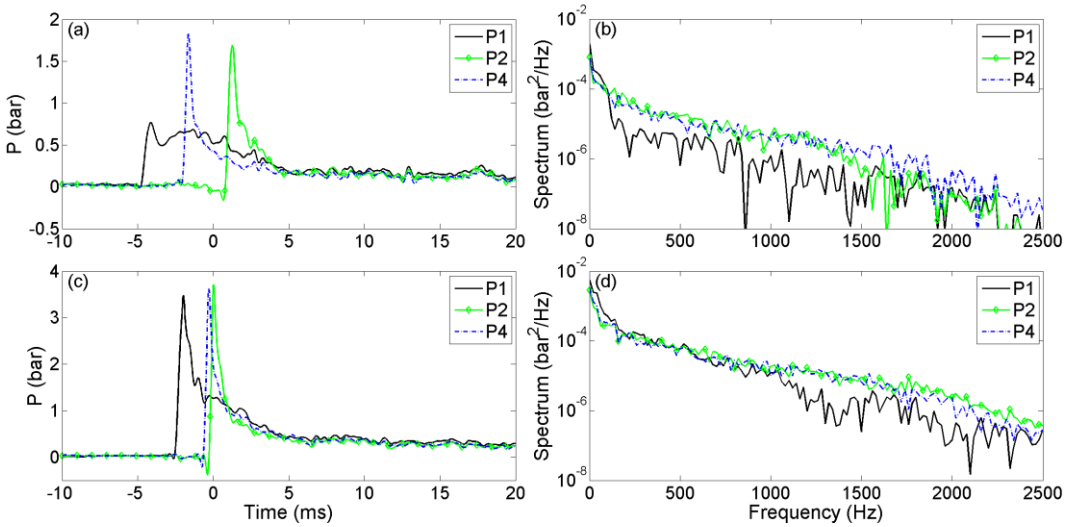

Figure 10: Oscillations in pressure (left plots) and their spectra (right plots) under impact in aerated water β = 1.62 %: (a, b) v = 4.12 m/s; (c, d) v = 7.0 m/s. Mass of the impact plate m = 52 kg.

3.3 Impact pressures and slamming force

Maximum pressures at the measured locations P1-P8 for impacts in pure and aerated water are presented in Figure 11(a,b) for (a) 32 kg and (b) 52 kg plates, respectively. It is shown that the impact pressures in pure water (the black circles in plots) are much higher than those measured in aerated water of 0.8 %, 1 % and 1.6 % void fraction. With the presence of air in the water the impact pressure decreases significantly in comparison with that in pure water. For example, for an impact velocity of 7 m/s and mass of 52 kg, the impact pressure in pure water $P1_{max}$ = 33.23 bar is reduced to that of 4.45 bar when the water has an aeration level of 1.6 %. This shows that aeration plays an important role during impact and can reduce impact pressure significantly. In addition, the water surface distortion also affects the impact pressures for the tests in aerated water. The water surface was disturbed by the bubble generation system, and so the impacts in aerated water were not as perfectly uniform across the surface of the plate as they were in pure water. This water surface distortion has a similar effect of reducing impact pressure in aerated water as found by others for plates with small deadrise angle (Chuang, 1966a; Lewison, 1969; Van Nuffel et al., 2014).

Maximum forces in pure and aerated water are presented in Figure 11(c,d) for the tested plates (m = 32 kg and 52 kg). There is a significant reduction in the impact force from tests conducted in pure water in comparison with those conducted in aerated water. Figure 12 shows the maximum force versus void fraction (β) of the water for the plates of mass 32 kg and 52 kg. Within the range of the experimental data in the present study, the maximum force appears to be an exponential function of the void fraction, given by:

$$F_{\max} = k_F e^{n\beta} \qquad (3)$$

in which coefficients k_F and n are estimated using a nonlinear least-squares fit to the experimental data. The fitted curves and the coefficient values are presented in each plot of Figure 12 for each impact velocity. The curves in Figure 12 show a similar tendency to the experimental results of Bullock et al. (2001) and simulations by Ma et al. (2016), in that there is significant reduction of the impact pressures due to a relatively small air content and that the effect of aeration increases with the violence of the impact. The reduction of wave impact pressure due to aerated water can be also found in Chuang et al. (2018) for wall impingement event in their study, where the wall impingement event is when a plunging breaking wave impinged on the frontal vertical wall of a fixed platform and aerated water was generated due to wave broken.

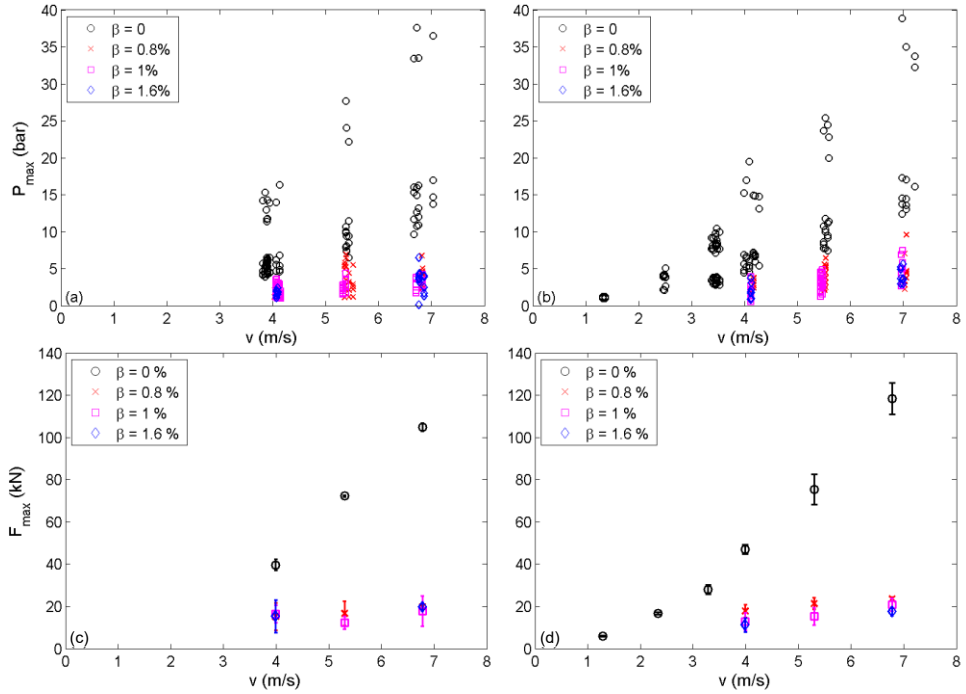

Figure 11: Impact pressures and force in pure and aerated water: (a,c) m = 32 kg; (b,d) m = 52 kg.

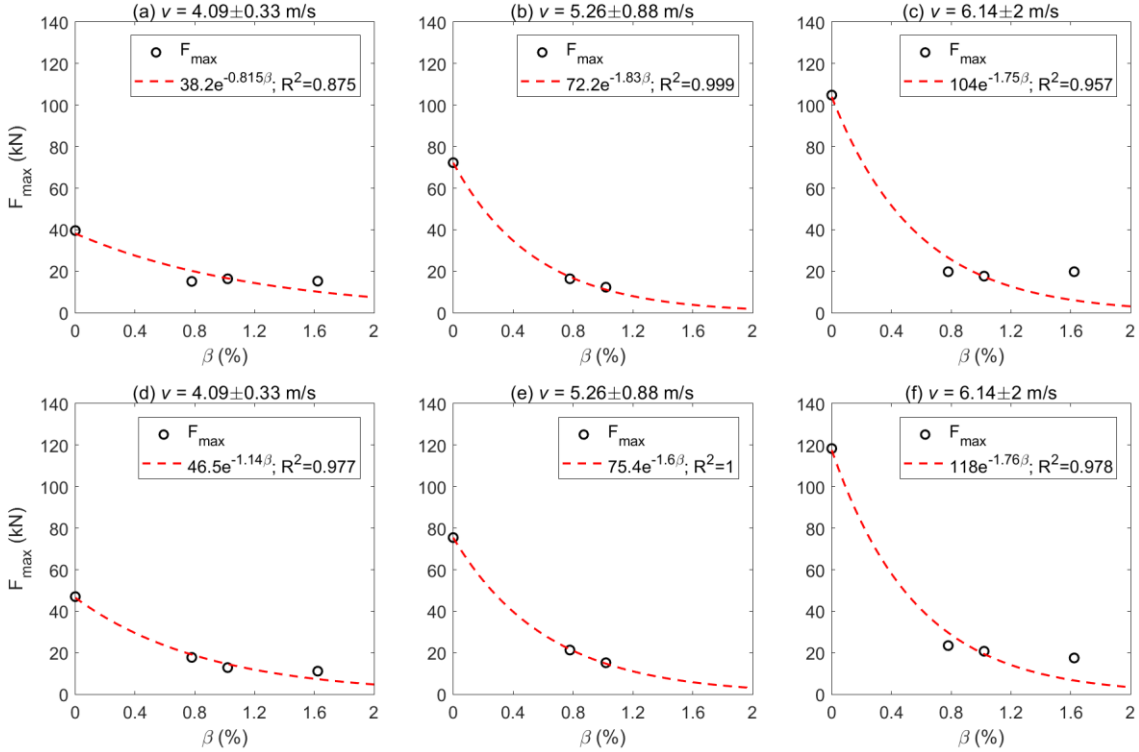

Figure 12: Impact force as a function of void fraction β: (a,b,c) m = 32 kg; (d,e,f) m = 52 kg.

3.4 Impulses of pressure and slam force

Impulse values can be obtained by integrating force or pressure over the duration of the impact. The first impulse (I^{first}) of the impact is defined as the impulse of the first positive phase of the impact, i.e. the area A1 in Figure 13 and the total impulse (I^{total}) is integrated from the start of the impact until the signal falls back to the noise level, i.e. the sum of the areas A1 to A7 in Figure 13. The "total impulse" for the drop tests is calculated for a duration from the start time of an impact until the time when the impact plate was restrained by the rope used to stop the plate falling onto the basin floor. Therefore, the "total impulse" used in this analysis does not consider the entire motion of the object brought to rest and therefore there may be a difference between the total impulses for various impacts.

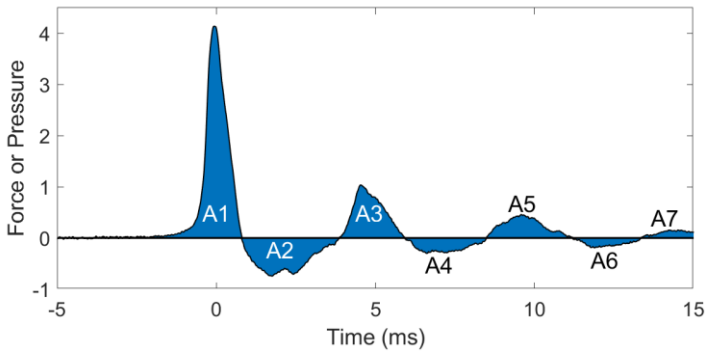

Figure 13: Definition sketch for the first impulse (I^{first}) and total impulse (I^{total}).

Pressure impulses of the plate impact in pure and aerated water are presented in Figure 14. The first pressure impulses (I_P^{first}) of the impact in pure water are much higher than those in aerated water and there is a linear relationship between the first impulse and the violence of the flow, as described by the impact velocity (Figure 14a,b). In pure water, scatter of the first pressure impulse is much smaller than the scatter of the impact pressures P_{max} presented in Figure 11(a,b). This smaller scatter of the first pressure impulse was also found from the experimental work by Zhu (1995). In contrast, variation of the first pressure impulse is still large for aerated water, similar to the variation of the impact pressures (Figure 11a,b). The total pressure impulses (I_P^{total}) are presented in Figure 14(c,d) and the variation of the total pressure impulse in pure water is as large as the variation in aerated water. There is no reduction of the total pressure impulses from pure water to aerated water for impacts of both 32 kg and 52 kg plates.

Figure 15 presents the first positive phase force impulse (I_F^{first}) and the total force impulse (I_F^{total}). Similar to the first pressure impulses in pure water (Figure 14a,b), the first force impulses are significantly larger than those in aerated water (Figure 15a,b). In pure water, the variation of the first force impulse is larger than the variation of the first pressure impulse, especially at high impact velocities from 4 m/s to 7 m/s (see Figure 14a,b and Figure 15a,b). Bullock et al. (2007) also presented experimental data that exhibited large variation in the first force impulse wave impact. The total force impulses in pure and aerated water are more or less the same, except the impacts of the 52 kg plate show the total force impulses in aerated water are higher than those in pure water (see Figure 15d).

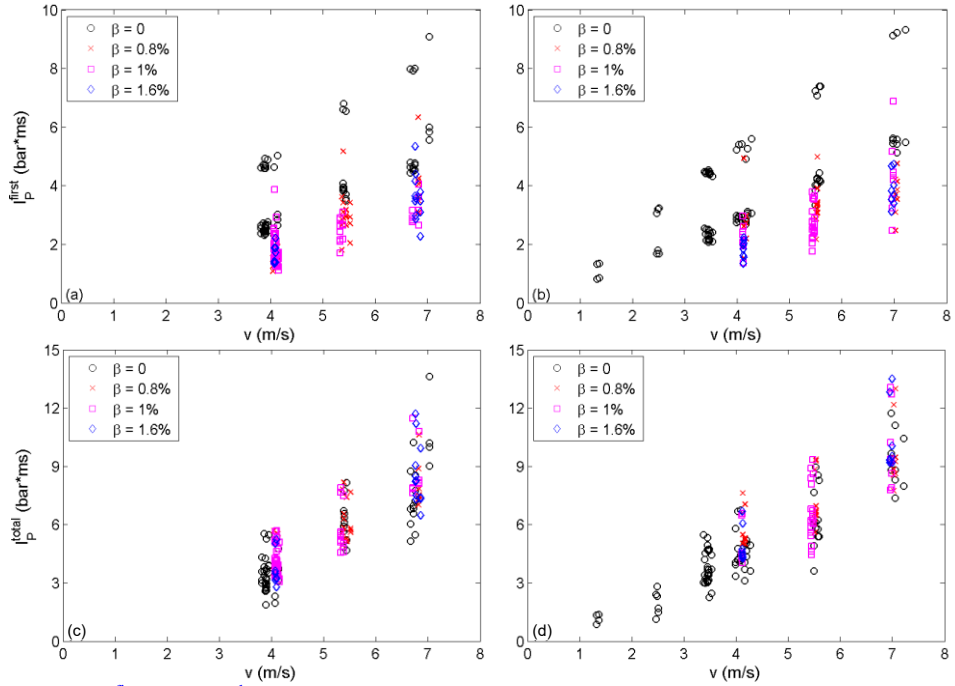

Figure 14: I_P^{first} and I_P^{total} of impact in pure and aerated water: (a,c) m = 32 kg; (b,d) m = 52 kg.

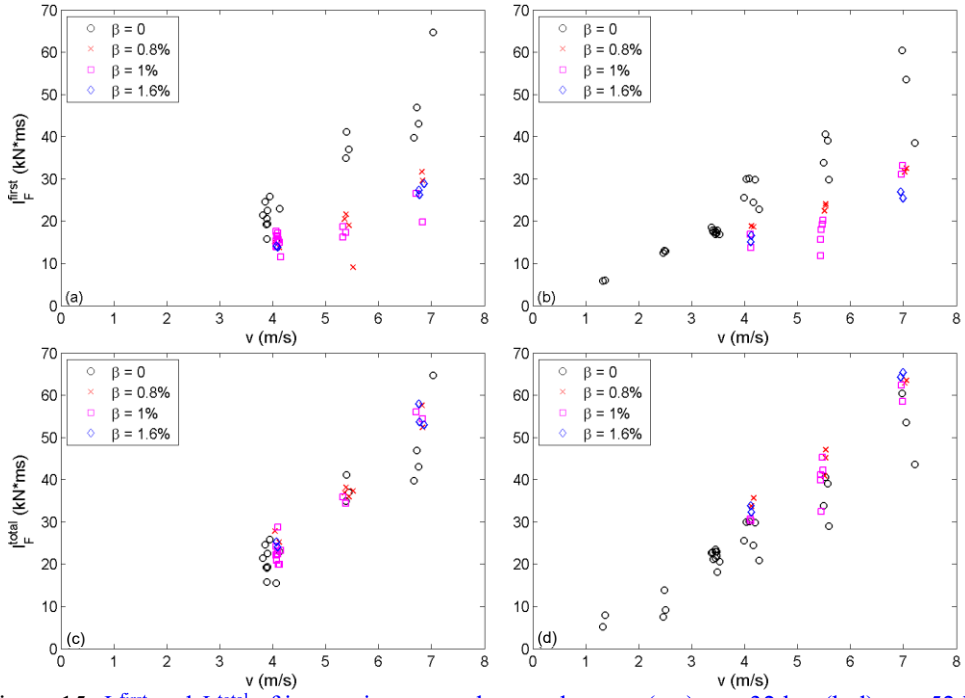

Figure 15: I_F^{first} and I_F^{total} of impact in pure and aerated water: (a,c) m = 32 kg; (b,d) m = 52 kg.

4 Conclusions

This paper presents results of an experimental campaign on the role of aeration in slamming impacts. Such impacts can have both local and global effects on offshore structures and ships, and may cause local damage and/or structural vibrations. The experiment was conducted by means of a free-falling rigid flat plate onto pure and aerated water surfaces, designed to represent severe slamming impacts with zero degree deadrise angle. The following conclusions should be useful in the context of local and global loads on offshore structures and ships, which need to be assessed as part of the marine structure design process. Currently, design codes do not include the effect of aeration and here we make observations of the implications for design.

Impacts in pure water

Physical modelling of slamming impacts by freely dropping a flat plate onto a pure water surface has enabled characterisation of the spatial distribution of impact pressures and its variation with impact velocity. The largest maximum pressure was found to occur at the centre of the plate, while the maximum pressure at locations near the edges is about 80 % of the pressure at the centre of the plate for v < 2 m/s and about 40 % for v > 2 m/s. In addition, the impact loadings on the tested plate are proportional to the square of the impact velocity and the empirical factors of this relationship are found to depend on the body mass and the location on the plate. These empirical coefficients may be considered as a reference for marine structure design if the effect of aeration is assessed for slamming impacts.

Post-impact, high frequency oscillations of pressures were observed, and these are due to repeated compression and expansion of the trapped air between the impact plate and water surface. These high frequency oscillations may need to be assessed for the fatigue analysis of a section of the hull or whole ship structure.

Effects of aeration on impacts

Aeration has an important effect on slamming impacts. There is a significant reduction in the hydrodynamic impact loadings (pressure and force) for those measured in aerated water compared to those in pure water. This reduction is not only due to the presence of air in the body of water, but also due to the water surface distortion. In addition, significant reductions in the pressure and force impulses of the first positive phase are also found from the slamming impacts in aerated water

compared with pure water, but there is almost no reduction of the total loading impulses. The variation of impulsive loadings is less sensitive than the peak loadings for slamming impacts. Therefore, the implication for design is that maximum instantaneous loads calculated for pure water may be conservative in the presence of aerated water. This is particularly important for offshore structures, where the wave impact often occurs in seas where wave breaking is commonplace and the water is likely to be considerably aerated before it impacts the structure. This is not yet taken into account in standard design practice (Det Norske Veritas, 2012&2016), but the loading amplitude and its spatial/temporal evolution is fundamental to the analysis of structural response, and thus it is recommended from the findings here that the aeration effects on slamming should be considered.

An exponential relationship of the maximum force and the void fraction has been empirically proposed with its coefficients found from the slamming impacts. These empirical coefficients may be considered as a reference for marine structure design if the effect of aeration is assessed for slamming impacts.

Acknowledgements

This study was a part of the FROTH (Fundamentals and Reliability of Offshore sTructure Hydrodynamics) project supported by the Engineering and Physical Science Research Council (EPSRC Grant EP/J012866/1). The FROTH project was led by Plymouth University and the collaborative partners included Oxford University, University of Bath, City University London and the Manchester Metropolitan University. The authors gratefully acknowledge the financial support provided by EPSRC and useful discussions with the project partners.

References

Alaoui A.E.M., Nême A., Tassin A., Jacques N., (2012). "Experimental study of coefficients during vertical water entry of axisymmetric rigid shapes at constant speeds." *Applied Ocean Research* **37**(0): 183-197.

Alaoui A.E.M., Nême A., Scolan Y.M. (2015). "Experimental investigation of hydrodynamic loads and pressure distribution during a pyramid water entry." *Journal of Fluids and Structures* **54**(0): 925-935.

Blanchard, D. C., and Woodcock, A. H. (1957). "Bubble formation and modification in the sea and its meteorological significance." *Tellus,* **9,** 145-158.

Bullock, G. N., Crawford, A. R., et al. (2001). "The influence of air and scale on wave impact pressures." *Coastal Engineering* **42**(4): 291-312.

Chan, E-S (1994). "Mechanics of deep water plunging-wave impacts on vertical structures." *Coast Eng* **22**:115-133.

Chanson, H. (1997). "Air bubble entrainment in free-surface turbulent shear flows." Academic Press, London, UK, 401 pp.

Chanson, H., S.-i. Aoki, et al. (2002). "Unsteady air bubble entrainment and detrainment at a plunging breaker: dominant time scales and similarity of water level variations." *Coastal Engineering* **46**(2): 139-157.

Chuang, S.-L. (1966a). "Slamming of rigid wedge-shaped bodies with various deadrise angles." David Taylor Model Basin, Washington DC, Report 2268.

Chuang, S.-L. (1966b). "Experiments on flat-bottom slamming", *Journal of Ship Research*, **10**(1), 10-17.

Chuang, WL., Chang, KA. & Mercier, R. (2017). "Impact pressure and void fraction due to plunging breaking wave impact on a 2D TLP structure." *Exp Fluids* **58**:68.

Chuang, WL., Chang, KA. & Mercier, R. (2018). "Kinematics and dynamics of green water on a fixed platform in a large wave basin in focusing wave and random wave conditions." *Exp Fluids*, **59**:100

Deane, G. B. and M. D. Stokes (1999). "Air Entrainment Processes and Bubble Size Distributions in the Surf Zone." *Journal of Physical Oceanography* **29**(7): 1393-1403.

Detsch, R., & Harris, I. (1989). "Dissolution and rise velocity of small air bubbles in water and salt water." *In OCEANS'89. Proceedings IEEE*, Vol. **1**, pp. 286-291.

Det Norske Veritas (2012). “Structural Design of Offshore Ships.” *Offshore Standard DNV-OS-C102*.
Det Norske Veritas (2014). “Environmental Conditions and Environmental Loads.” Recommended Practice DNV-RP-C205.
Det Norske Veritas (2016). “Hull structural design – Ships with length 100 meters and above.” Rules for Classifications of Ships, Part 3, Chapter 1.
Ermanyuk, E.V. and M. Ohkusu (2005). “Impact of a disk on shallow water.” *Fluids and Structures* **20(**3): 345-357. http://doi.org/10.1016/j.jfluidstructs.2004.10.002.
Faltinsen, O. (1993). *Sea Loads on Ships and Offshore Structure* (Cambridge University Press).
Faltinsen, O. (2000). "Hydroelastic slamming." *Journal of Marine Science and Technology* **5**(2): 49-65. http://dx.doi.org/10.1007/s007730070011.
Faltinsen, O., M. Landrini, et al. (2004). "Slamming in marine applications." *Journal of Engineering Mathematics* **48**(3-4): 187-217.
Franz, G. J. (1959). “Splashes as sources of sound in liquids.” *J. Acoust. Soc. Amer.,* **31,** 1080-1096.
Kapsenberg, G. K. (2011). “Slamming of ships: Where are we now?,” *Philos. Trans. R. Soc., A* **369**, 2892–2919. http://dx.doi.org/10.1098/rsta.2011.0118.
Kay, J. (2014). “UK storms destroy railway line and leave thousands without power,” BBC News, available at http://www.bbc.co.uk/news/uk-26042990.
Kwon, S.H., Jung, D.J. et al. (2003). “An Alternative Experiment for Slamming Using an Air Pressure Cylinder.” *Proceeding of the 13th International Offshore and Polar Engineering Conference (ISOPE)*, Honolulu, Hawaii, USA, pp. 542-548.
Lang, N. A., Rung, T. (2011). “Impact Tests in Pure and Aerated Water.” *Proceeding of the 30th International Conference on Ocean, Offshore and Arctic Engineering* (OMAE), Rotterdam, The Netherlands, June 19–24.
Lewison, G., Maclean, W. M. (1968). “On the cushioning of water impact by entrapped air.” *Journal of Ship Research*, **12**(2), 116-130.
Liger-Belair, G., Marchal, R., Robillard, B., Dambrouck, T., Maujean, A., Vignes-Adler, M. and Jeandet, P. (2000). “On the Velocity of Expanding Spherical Gas Bubbles Rising in Line in Supersaturated Hydroalcoholic Solutions: Application to Bubble Trains in Carbonated Beverages.” *Langmuir* **16** (4), 1889-1895. DOI: 10.1021/la990653x
Longuet-Higgins, M. S. (1993). “Bubble noise mechanisms - A review”. *Natural Physical Sources of Underwater Sound,* B. R. Kerman, Ed., Kluwer Academic, 419–452.
Ma, Z. H., Causon, D. M., Qian, L., Mingham, C. G., Mai, T., Greaves, D. & Raby, A. (2016). "Pure and aerated water entry of a flat plate." *Physics of Fluids* **28**(1): 016104. DOI: http://dx.doi.org/10.1063/1.4940043
Mai, T. (2017). “On the role of aeration, elasticity and wave-structure interaction on hydrodynamic impact loading.” *PhD thesis at Plymouth University*. http://hdl.handle.net/10026.1/9884
Mai, T., Greaves, D., Raby, A. (2014). “Aeration effects on impact: Drop test of a flat plate.” *Proc. of 24th International Ocean and Polar Engineering Conference*, Busan, Republic of Korea, June 15-20, 703-709.
Medwin, H. (1977). "In situ acoustic measurements of microbubbles at sea." *Journal of Geophysical Research* **82**(6): 971-976.
Melville, W. K. (1996). “The role of surface-wave breaking in air-sea interaction.” *Annu. Rev. Fluid Mech.,* **28,** 279–321.
Minnaert, M. (1933). “On musical air-bubbles and the sounds of running water.” *Philos. Mag.,* **16,** 235–248.
Monahan, E. C. (1993). “Occurrence and evolution of acoustically relevant sub-surface bubble plumes and their associated, remotely monitorable, surface whitecaps.” *Natural Physical Sources of Underwater Sound,* B. R. Kerman, Ed., Kluwer Academic, 503-517.
Rodgers, L. and Bryson, M. (2014). “10 key moments of the UK winter storms,” BBC News, available at http://www.bbc.co.uk/news/uk-26170904.

Rubin, B. D. (1999). "The basics of competitive diving and its injuries," Clin. Sports Med. **18**, 293–303.

Oh, S. H. , Kwon, S. H., et al. (2009), "A close look at air pocket evolution in flat impact." *Proc. of 24th International Workshop on Water Waves and floating Bodies*, Zelenogorsk, Russia.

Pumphrey, H. C., and Elmore, P. A. (1990). "The entrainment of bubbles by drop impacts". *J. Fluid Mech.,* **220,** 539–567.

Smith, N. J., Stansby, P. K., et al. (1998). "The slam force on a plate in free flight due to impact on a wave crest". *Journal of Fluids and Structures*, vol. 12, 183-196.

Van Nuffel, D., K. Vepa, et al. (2013). "A comparison between the experimental and theoretical impact pressures acting on a horizontal quasi-rigid cylinder during vertical water entry." *Ocean Engineering*.

Verhagen, J.H.G. (1967). "The impact of a flat plate on a water surface." *Journal of Ship Research* **10**, 211–223.

von Karman, T. (1929). "The impact on seaplane floats during landing." National Advisory Committee for Aeronautics. *Technical Note*, vol. 321.

Wagner, H. (1932). "Über Stoß- und Gleitvorgänge an der Oberfläche von Flüssigkeiten." *ZAMM - Journal of Applied Mathematics and Mechanics / Zeitschrift für Angewandte Mathematik und Mechanik* 12(4): 193-215.

Wilson, W. D. (1960). "Speed of Sound in Sea Water as a Function of Temperature, Pressure, and Salinity." *The Journal of the Acoustical Society of America* **32**(6): 641-644.

Wood, I.R. (1991). "Air entrainment in free-surface flows." IAHR Hydraulic Structures Design Manual No. **4**, Hydraulic Design Considerations. Balkema, Rotterdam, The Netherlands, 149 pp.

Zhao, R., Faltinsen, O. and Aarsnes, J. (1996). "Water Entry of Arbitrary Two-Dimensional Sections with and without Flow Separation." *Proceedings of the 21st Symposium on Naval Hydrodynamics*, National Academy Press, Washington DC, 408-423.

Zhu, L. (1995). "Structural Response of Ship Plates in Slamming-Drop Test Results and Analysis", University of Glasgow, Department of Naval Architecture and Ocean Engineering-Reports-NAOE.